

# 1 Improved chemistry restraints for crystallographic refinement by integrating 2 the Amber force field into Phenix

3 Authors

4 Nigel W. Moriarty<sup>a\*</sup>, Pawel A. Janowski<sup>b1</sup>, Jason M. Swails<sup>b</sup>, Hai Nguyen<sup>b</sup>, Jane S.

5 Richardson<sup>c</sup>, David A. Case<sup>a</sup> and Paul D. Adams<sup>ad</sup>

6 <sup>a</sup>Molecular Biosciences and Integrated Bioimaging, Lawrence Berkeley National Laboratory,  
7 Berkeley, California, 94720-8235, USA

8 <sup>b</sup>Department of Chemistry & Chemical Biology, Rutgers University, Piscataway, NJ, 08854, USA

9 <sup>c</sup>Department of Biochemistry, Duke University, Durham, NC, 27710, USA

10 <sup>d</sup>Department of Bioengineering, University of California at Berkeley, Berkeley, CA, 94720, USA

11 Correspondence email: [NWMoriarty@LBL.Gov](mailto:NWMoriarty@LBL.Gov)

12 <sup>1</sup>Currently at Microsoft

13 **Funding information** National Institutes of Health (grant No. GM122086 to David A. Case; grant No.  
14 P01GM063210 to Paul D. Adams, Jane S. Richardson); Department of Energy (grant No. DE-AC02-  
15 05CH11231 to Lawrence Berkeley National Laboratory).

16 **Synopsis** The full Amber force field has been integrated into Phenix as an alternative refinement  
17 target. With a slight loss in speed, it achieves improved stereochemistry, fewer steric clashes and  
18 better hydrogen bonds.

19 **Abstract** The refinement of biomolecular crystallographic models relies on geometric restraints to  
20 help address the paucity of experimental data typical in these experiments. Limitations in these  
21 restraints can degrade the quality of the resulting atomic models. Here we present an integration of the  
22 full all-atom Amber molecular dynamics force field into Phenix crystallographic refinement, which  
23 enables a more complete modeling of biomolecular chemistry. The advantages of the force field  
24 include a carefully derived set of torsion angle potentials, an extensive and flexible set of atom types,  
25 Lennard-Jones treatment of non-bonded interactions and a full treatment of crystalline electrostatics.  
26 The new combined method was tested against conventional geometry restraints for over twenty-two  
27 thousand protein structures. Structures refined with the new method show substantially improved  
28 model quality. On average, Ramachandran and rotamer scores are somewhat better; clash scores and  
29 MolProbity scores are significantly improved; and the modelling of electrostatics leads to structures  
30 that exhibit more, and more correct, hydrogen bonds than those refined with traditional geometry  
31 restraints. We find in general that model improvements are greatest at lower resolutions, prompting  
32 plans to add the Amber target function to real-space refinement for use in electron cryo-microscopy.  
33 This work opens the door to the future development of more advanced applications such as Amber-

34 based ensemble refinement, quantum mechanical representation of active sites and improved  
35 geometric restraints for simulated annealing.

36 **Keywords: Amber refinement target; H-bond quality; Amber in Phenix; C $\beta$  deviations; peptide**  
37 **orientations**

## 38 **1. Introduction**

39 Accurate structural knowledge lies at the heart of our understanding of the biomolecular function and  
40 interactions of proteins and nucleic acids. With close to 90% of structures in the Protein Data Bank  
41 (Berman *et al.*, 2000) solved via x-ray diffraction methods, crystallography is currently the pre-  
42 eminent method for determining biomolecular structure. Crystal structure refinement is a  
43 computational technique that plays a key role in post-experiment data interpretation. Refinement of  
44 atomic coordinates entails solving an optimization problem to minimize the residual difference  
45 between the experimental and model structure factor amplitudes (Jack & Levitt, 1978; Agarwal, 1978;  
46 Murshudov *et al.*, 1997). However, due to inherent experimental limitations and a typically low data  
47 to parameter ratio, the employment of additional restraints, commonly referred to as geometry or  
48 steric restraints, is key to successful structural refinement (Waser, 1963). These restraints, which can  
49 be thought of as a prior in the Bayesian sense, provide additional observations in the optimization  
50 target and reduce the danger of overfitting. Their use leads to higher quality, more chemically  
51 accurate models.

52 Most current refinement programs (Afonine *et al.*, 2012; Murshudov *et al.*, 2011; Sheldrick, 2008;  
53 Bricogne *et al.*, 2011) employ a set of covalent-geometry restraints first proposed by Engh & Huber in  
54 1991 and later augmented and improved in 2001 (Engh & Huber, 1991, 2001). This set of restraints is  
55 based on a survey of accurate high-resolution small molecule crystal structures from the Cambridge  
56 Structural Database (Groom *et al.*, 2016) and includes restraints on interatomic bond lengths, bond  
57 angles and  $\omega$  torsion angles. In addition, parameters are added to enforce proper chirality and  
58 planarity; multiple-minimum targets for backbone and side chain torsion angles; and repulsive terms  
59 to prevent steric overlap between atoms. Those terms are defined from small-molecule and high-  
60 resolution macromolecular crystal structure data and from interaction-specified van der Waals radii.  
61 They are very similar but not identical between refinement programs.

62 The Engh & Huber restraints function reasonably well, while the additional terms have been gradually  
63 improved, but a number of limitations have been identified over the years. Some of these limitations  
64 include: a lack of adjustability to differences in local conformation, protonation, and hydrogen  
65 bonding and to their changes during refinement; incomplete or inaccurate atom types and parameters  
66 for ligands, carbohydrates, and covalent modifications; use only of repulsive and not attractive steric  
67 terms; omission of explicit hydrogen atoms and their interactions; misleading targets resulting from  
68 experimental averaging artifacts; inaccurate dihedral restraints; and lack of awareness of electrostatic

69 and quantum dispersive interactions with a consequent lack of accounting for hydrogen bonding  
70 cooperativity (Priestle, 2003; Touw & Vriend, 2010; Davis *et al.*, 2003; Moriarty *et al.*, 2014; Tronrud  
71 *et al.*, 2010).

72 Phenix (Adams *et al.*, 2010) includes a built-in system for defining ligand parameters (Moriarty *et al.*,  
73 2009) that by default restrains the explicit hydrogen atoms at electron-cloud-center positions for X-ray  
74 and optionally at nuclear positions for neutron crystallography (Williams, Headd *et al.*, 2018).

75 Addition of the Conformation Dependent Library (CDL) (Moriarty *et al.*, 2014), which makes  
76 backbone bond lengths and angles dependent on  $\phi, \psi$  values, has improved the models obtained from  
77 refinement at all resolutions, and thus is the default in Phenix refinement (Moriarty *et al.*, 2016).

78 Similarly, Phenix uses ribose-pucker and base-type dependent torsional restraints for RNA (Jain *et al.*,  
79 2015). For bond lengths and angles, protein side chains continue to use standard Engh & Huber  
80 restraints while RNA/DNA use early values (Gelbin *et al.*, 1996; Parkinson *et al.*, 1996) with a few  
81 modifications. This use of combined restraints is here designated CDL/E&H.

82 An alternative approach is the use of geometry restraints based on all-atom force fields used for  
83 molecular dynamics studies. This is not a novel idea. In fact, some of the earliest implementations of  
84 refinement programs employed molecular mechanics force fields (Jack & Levitt, 1978; Brünger *et al.*,  
85 1987, 1989). However, at the time, restraints derived from coordinates of ideal fragments (Tronrud *et al.*,  
86 1987; Hendrickson & Konnert, 1980) were found to provide better refinement results. The  
87 insufficiency of molecular mechanics-based restraints was mainly attributed to two factors: inaccurate  
88 representation of chemical space because of too few atom types, and biases in conformational  
89 sampling resulting from unshielded electrostatic interactions. Subsequently, however, the methods of  
90 molecular dynamics and corresponding force fields have seen significant development and  
91 improvement. Current force fields contain more atom types and are easily adjustable as needed. They  
92 are typically parameterized against accurate quantum mechanical calculations, not feasible just a few  
93 years ago, as well as using more representative experimental results. Significant methodological  
94 advances, such as the development of Particle Mesh Ewald (York *et al.*, 1993; Darden *et al.*, 1993) for  
95 accurate calculation of crystalline electrostatics and improved temperature and pressure control  
96 algorithms, have greatly increased accuracy. Modern force fields have been shown to agree well with  
97 experimental data (Zagrovic *et al.*, 2008; van Gunsteren *et al.*, 2008; Showalter & Brüschweiler,  
98 2007; Grindon *et al.*, 2004; Bowman *et al.*, 2011), including crystal diffraction data (Cerutti *et al.*,  
99 2009; Janowski *et al.*, 2013; Cerutti *et al.*, 2008; Liu *et al.*, 2015; Janowski *et al.*, 2015).

100 We have made it possible to use of the Amber molecular mechanics force field as an alternative  
101 source of geometry restraints to those of CDL/E&H. Here we present an integration of the Phenix  
102 software package for crystallographic refinement, *phenix.refine* (Afonine *et al.*, 2012) and the Amber  
103 software package (Case *et al.*, 2018) for molecular dynamics. We present results of paired refinements  
104 for 22,544 structures and compare Amber to traditional refinement in terms of model quality,

105 chemical accuracy and agreement with experimental data, studied both for overall statistics and for  
106 representative individual examples. We also describe the implementation and discuss future  
107 directions.

## 108 **2. Methods**

### 109 **2.1. Code preparation**

110 The integration of the Amber code into *phenix.refine* uses a thin client. Amber provides a python API  
111 to its *sander* module, so that a simple "import sander" python command allows Phenix to obtain  
112 Amber energies and forces through a method call. At each step of coordinate refinement, Phenix  
113 expands the asymmetric unit coordinates to a full unit cell (as required by *sander*), combines energy  
114 gradients returned from Amber (in place of those from its internal geometric restraint routines) with  
115 gradients from the X-ray target function, and uses these forces to update the coordinates, either by  
116 minimization or by simulated annealing molecular dynamics. Alternate conformers take advantage of  
117 the "locally-enhanced-sampling" (LES) facility in *sander*: atoms in single-conformer regions interact  
118 with multiple-copy regions via the average energy of interaction, while different copies of the same  
119 group do not interact among themselves (Roitberg & Elber, 1991; Simmerling *et al.*, 1998).

120 The Amber files required are created by a preliminary *AmberPrep* program that takes a PDB file as  
121 input. It creates both a parameter-topology (*prmtop*) file used by Amber and a new PDB file  
122 containing a complete set of atoms (including hydrogens and any missing atoms) needed to do force  
123 field calculations. Alternate conformers, if present in the input PDB file, are translated into *sander*  
124 LES format. For most situations, *AmberPrep* does not require the user to have any experience with  
125 Amber or with molecular mechanics; less-common situations (described below) require some  
126 familiarity with Amber. All the code required for both the *AmberPrep* and *phenix.refine* steps is  
127 included in the current major release, 1.16-3549 and subsequent nightly builds of Phenix.

### 128 **2.2. Structure selection and overall refinement protocol**

129 To compare refinements using Amber against traditional refinements with CDL/E&H restraints,  
130 structures were selected from the Protein Data Bank (Burley *et al.*, 2019) using the following criteria.  
131 Entries must have untwinned experimental data available that are at least 90% complete. Each entry's  
132  $R_{\text{free}}$  was limited to a maximum of 35%,  $R_{\text{work}}$  to 30% and the  $\Delta R$  ( $R_{\text{free}} - R_{\text{work}}$ ) to a minimum of 1.5%.  
133 The lowest resolution was set at 3.5Å. Entries containing nucleic acids were excluded.

134 Coordinate and experimental data files were obtained directly from the Protein Data Bank (PDB) and  
135 inputs prepared via the automated *AmberPrep* program (see section 2.1 above). Entries containing  
136 complex ligands were included if the file preparation program *AmberPrep* was able to automatically  
137 generate and include the ligand geometry data. Details of the internals of *AmberPrep* will be  
138 described elsewhere. Resolution bins (set at 0.1Å) with less than 10 refinement pairs were eliminated

139 to reduce noise caused by limited statistics. Complete graphs are included in the supplemental  
140 material. The resulting 22,000+ structures had experimental data resolutions between 0.5Å and 3.2Å,  
141 with most of the structures in the 1.0-3.0 Å range (see figure 1).

142 Each model was then subjected to 10 macrocycles of refinement using the default strategy in  
143 *phenix.refine* for reciprocal space coordinate refinement, with the exception that real space refinement  
144 was turned off. By default, the first macrocycle uses a least-squares target function and the rest use  
145 maximum likelihood. Other options included optimization of the weight between the experimental  
146 data and the geometry restraints. This protocol was performed in parallel, once using CDL/E&H and  
147 once using Amber geometry restraints. In addition, Cβ pseudo-torsion restraints were not included in  
148 the restraints model. Only one copy of each alternate conformation was considered initially (i.e.  
149 alternative location A). The quality of the resulting models was assessed numerically using  
150 MolProbity (Williams, Headd *et al.*, 2018) available in Phenix (Adams *et al.*, 2010), by *cpptraj* (Roe  
151 & Cheatham, 2013) available in *AmberTools* (Case *et al.*, 2018) and by visual inspection with electron  
152 density and validation markup in KiNG (Chen *et al.*, 2009). All-atom dots for figure 10 were counted  
153 in Mage (Richardson & Richardson, 2001) and figures 5-9 were made in KiNG. To avoid  
154 typographical ambiguity, PDB codes are given here with lower case for all letters except L (e.g.,  
155 1nLs).

### 156 **2.3. Weight factor details**

157 The target function optimized in *phenix.refine* reciprocal space atomic coordinate refinement is of the  
158 general form:

$$T_{xyz} = w * T_{exp} + T_{xyz\_restraints}$$

159 where all the terms are functions of the atomic coordinates,  $T_{xyz}$  is the target residual to be minimized,  
160  $T_{exp}$  is a residual between the observed and model structure factors and quantifies agreement with  
161 experimental data,  $T_{xyz\_restraints}$  is the residual of agreement with the geometry restraints and  $w$  is a scale  
162 factor that modulates the relative weight between the experimental and the geometry restraint terms.  
163 In traditional refinement  $T_{xyz\_restraints}$  is calculated using the set of CDL/E&H restraints:

$$T_{xyz} = w * T_{exp} + T_{CDL/E\&H}$$

164 To implement Phenix-Amber we substitute this term with the potential energy calculated using the  
165 Amber force field:

$$T_{xyz} = w * T_{exp} + E_{AmberFF}$$

166 where the Amber term is intentionally represented now by an  $E$  to emphasize that we directly  
167 incorporate the full potential energy function calculated in Amber using the ff14SB (Maier *et al.*,  
168 2015) force field.

169 In a standard default Phenix refinement, the weight,  $w$ , is a combination of a value based on the ratio  
170 of gradient norms (Brünger *et al.*, 1989; Adams *et al.*, 1997) and a scaling factor that defaults to  $\frac{1}{2}$ .  
171 This initial weight can be optimized using a procedure described previously (Afonine *et al.*, 2011).  
172 This procedure uses the results of ten refinements with a selection of weights, considering the bond  
173 and angle rmsd, the R-factors and validation statistics to determine the best weight for the specific  
174 refinement at each of the ten macrocycles. The same procedure was used to estimate an optimal  
175 weight for the Phenix-Amber refinements. (If faster fixed-weight refinements are desired, we have  
176 found that a scaling factor of 0.2, rather than 0.5, scales the Amber gradients to be close to those from  
177 the CDL/E&H restraints, allowing the simpler, default, weighting scheme in *phenix.refine* to be used.)

### 178 3. Results

#### 179 3.1. Full-dataset score comparisons

180 On average, the Phenix-Amber combination produced slightly higher R-work and R-free (figure 2)  
181 but higher quality models (figure 3). The increase in R-factors is most pronounced in the 1.5–2.5 Å  
182 range. This is a result of the weight optimisation procedure having different limits for optimal weight  
183 in this resolution range. The increase was less for R-free than R-work such that the R-delta is less for  
184 refinements using Amber gradients. The Phenix-Amber refinements exhibited improved (lower)  
185 MolProbity scores and contained fewer clashes between atoms. Plots show the mean of the values in  
186 the 0.1 Å resolution bin as well as the 95% confidence level of the standard error of the mean (SEM).  
187 MolProbity clashscores are particularly striking: for refinement using CDL/E&H restraints,  
188 clashscores steadily increase as resolution worsens, often resulting in very high numbers of steric  
189 clashes. On the other hand, the mean clash-score with Amber restraints appears to be nearly  
190 independent of resolution and remains consistent at about 2.5 clashes per 1000 atoms across all  
191 resolution bins. The SEM range is non-overlapping for worse than 1 Å indicating that the Amber force  
192 field is producing better geometries at mid to low resolution. There are more favored Ramachandran  
193 points (backbone  $\phi, \psi$ ) and fewer Ramachandran outliers for the Phenix-Amber refinements. This  
194 difference is most marked for resolutions worse than 2 Å. Phenix-Amber refinement also improves  
195 (lowers) the number of rotamer outliers but doesn't differentiate via the SEM, and increases the  
196 proportion of hydrogen bonds. While the rotamer outlier results remain similar, the hydrogen bonding  
197 results have a large difference at worse than 1.5 Å resulting in nearly double the bonds near 3 Å.  
198 Common to all the plots is a change near 1.5 Å, where the weight optimisation procedure common to  
199 both CDL/E&H and Amber refinement loosens the weight on geometry restraints somewhat, to allow  
200 more deviations at resolutions where the data is capable of unambiguously showing them. Bond and  
201 angle rmsd comparison are less pertinent as the force fields do not have ideal values for  
202 parameterisations and comparing the Phenix-Amber bonds and angles to the CDL/E&H values is not

203 a universal metric. The curious can see the plots in figure S1. Overall, improvement with Amber is  
204 substantial in the lower resolution refinements.

205 Models refined with Phenix-Amber are more likely to exhibit electrostatic interactions such as H-  
206 bonds and salt links, as well as better van der Waals contacts. Though the resulting atom movements  
207 are generally small, these changes can be meaningful, especially when interpreting H-bonding  
208 networks or interaction distances at active sites.

209 One validation metric that is worse for Phenix-Amber refinements is the number of outliers of the C $\beta$   
210 positions. Both the mean and the SEM show clear differentiation. The C $\beta$  deviation gives a combined  
211 measure of distortion in the tetrahedron around the C $\alpha$  atom and with traditional E&H restraints it is  
212 quite robustly sensitive to incompatibility between how the backbone and side chain conformations  
213 have been modelled (Lovell *et al.*, 2003). For CDL/E&H refinements, however, the percentage of C $\beta$ d  
214 outliers (>0.25Å) is negligible for low and mid resolutions, only increasing to 0.2% at higher  
215 resolutions (see figure 4). This is in line with the CDL/E&H providing tight geometrical restraints out  
216 to C $\beta$  at most resolutions, but loosened somewhat at better than 1.5Å resolution where there is enough  
217 experimental information to move an angle away from ideal. Note that explicit C $\beta$  restraints were  
218 turned off for all Phenix refinements and that the Amber force field does not have an explicit C $\beta$  term;  
219 however, if all angles around the C $\alpha$  are kept ideal then the C $\beta$  position will also be ideal even if it is  
220 incorrectly positioned in the structure. The following section analyses specific local examples where  
221 output structures show differences for either the positive or the negative trends seen in the overall  
222 comparisons, in order to understand their nature, causes and meaning across resolution ranges.

### 223 **3.2. Examination of individual examples**

224 As noted above, in comparison with the CDL/E&H restraint refinements, the Phenix-Amber  
225 refinements have much higher percentages of C $\beta$  deviation outliers, increasing at the low-resolution  
226 end to more than 1% of C $\beta$  atoms. Amber refinement also has more bond length and angle outliers.

227 The following examines a sample of cases at high, mid and lower resolutions to understand the  
228 starting-model characteristics and refinement behavior that produce these differences.

#### 229 **3.2.1. High resolution: waters, alternates, C $\beta$ d outliers and atoms in the wrong peak**

230 In the high-resolution range (better than 1.7Å), it appears that the commonest problems not easily  
231 correctable by refinement are caused either by modeling the wrong atom into a density peak or by  
232 incorrect modeling, labeling, or truncation of alternate conformations. Such problems are usually  
233 flagged in validation either by all-atom clashes, by C $\beta$  deviations and sometimes by bad bond lengths  
234 and angles.

235 Figure 5a shows a case where a water molecule had been modeled in an electron density peak that  
236 should really be a nitrogen atom of the Arg guanidinium. CDL/E&H refinement (figure 5b) corrected

237 the bad geometry at the cost of moving the guanidinium even further out of density; Amber  
238 refinement changed the guanidinium orientation but made no overall improvement (figure 5c); all  
239 three versions have a bad clash. If the water were deleted, then either refinement method would  
240 undoubtedly do an excellent job (figure 5d). This type of problem is absent at low resolution where  
241 waters are not modeled but occurs quite often at both high and mid resolution, for other branched side  
242 chains, for Ile C $\delta$  (for example, 3js8 195) and even occasionally for Trp (e.g. 1qw9 B170).

243 C $\beta$  deviation outliers ( $\geq 0.25\text{\AA}$ ) are often produced by side chain alternates with quite different C $\beta$   
244 positions but no associated alternates defined along the backbone. Since the tetrahedron around C $\alpha$   
245 should be nearly ideal, that treatment almost guarantees bad geometry. The rather simple solution,  
246 implemented in Phenix, is to define alternates for all atoms until the i+1 and i-1 C $\alpha$  atoms – as in the  
247 "backrub" motion; (Davis *et al.*, 2006). PDB codes 1dy5, 1gwe and 1nLs each have a number of such  
248 cases. Figure 6a,b show 1nLs Ser 215, initially with an outlier C $\beta$ d, 0.49 $\text{\AA}$  distance between the two  
249 C $\beta$  atoms and a single C $\alpha$ . CDL/E&H refinement pulls the C $\beta$  atoms to be only 0.23 $\text{\AA}$  apart, avoiding  
250 a C $\beta$ d with only slightly worse fit to the density; Amber reduces the C $\beta$ d only slightly, but it does  
251 keep this flag of an underlying problem. When alternates are defined for the backbone peptides, both  
252 systems improve.

253 Worse cases occur where one or both alternates have been fit incorrectly as well as not being  
254 expanded along the backbone appropriately. Figure 6c shows Thr 196, with a huge C $\beta$ d of 0.88 $\text{\AA}$  (not  
255 shown) and very poor geometry, because altB was fit incorrectly (just as a shift of altA rather than as  
256 a new rotamer). This time even CDL/E&H refinement produces a C $\beta$ d outlier, but smaller than for  
257 Amber. Figure 6d shows the excellent Amber result after the misfit of altB was approximately  
258 corrected.

### 259 **3.2.2. Mid resolution: backward side chains and rare conformations**

260 An even commoner case at both high and mid resolutions where the wrong atom is fit into a density  
261 peak is a backward-fit C $\beta$ -branched residue, well illustrated by a very clear Thr example in 1bkr at  
262 1.1 $\text{\AA}$  (figure 7a). Thr 101 is a rotamer outlier (gold) on a regular  $\alpha$ -helix with a C $\beta$ d of 0.63 $\text{\AA}$ . The  
263 deposited Thr 101 also has a bond-angle deviation of 13.5 $\sigma$ ; clashes at the C $\gamma$  methyl; its C $\beta$  is out of  
264 density; O $\gamma$  is in the lower peak; and C $\gamma$  is in the higher peak. It is shown in figure 7 with 1.6 $\sigma$  and 4 $\sigma$   
265 2mF $_o$ -DF $_c$  contours (but without C $\beta$  deviation and angle markups for clarity). This mistake was not  
266 obvious because anisotropic B's were used too early in the modeling resulting in the Thr C $\beta$  being  
267 refined to a 6:1 aniso-axis ratio that covered both the modeled atom and the real position. The figures  
268 show the density as calculated with isotropic B factors.

269 Given this difficult problem for automated refinement, each of the two target functions reacts very  
270 differently. Both refinements still have the C $\gamma$  methyl clashing with a helix backbone CO in good



271 density, very diagnostic of a problem with the C $\gamma$ . It is indeed the wrong atom to have in that peak, as  
272 shown also by the relative peak heights. The CDL/E&H refinement (figure 7b) achieves tight  
273 geometry and a good rotamer, moving the C $\beta$  into its correct density peak, but pays the price for not  
274 correcting the underlying problem by swinging the O $\gamma$  out of density. The Amber refinement (figure  
275 7c) achieves an atom in each of the three side chain density peaks, but pays the price for not  
276 correcting the underlying problem by having the wrong chirality at the C $\beta$  atom. It still also has bond-  
277 angle outliers, which may be a sign of unconverged refinement.

278 The original PDB entry, the CDL/E&H refinement and the Amber refinement structures for Thr 101  
279 are all very badly wrong, but each in an entirely different way. The deposited model, 1bkr, looks very  
280 poor by traditional model validation, but has a misleadingly good density correlation, given the  
281 extremely anisotropic C $\beta$  B-factor. The CDL/E&H output looks extremely good on traditional  
282 validation except for the clashes and would show a lowered but still reasonable density correlation;  
283 however, it is the most obviously wrong upon manual inspection. The Amber output has clashes and  
284 currently has modest bond-angle outliers, but it fits the density very closely making it difficult to  
285 identify as incorrect by visual inspection. The problem could be recognized automatically by a simple  
286 chirality check. Shown in figure 7d, Thr 101 was rebuilt quickly in KiNG, with the **p** rotamer and a  
287 small backrub motion. Either Phenix-CDL/E&H or Phenix-Amber refinement would do a very good  
288 job from such a rough refit with the correct atoms near the right places.

289 At mid resolution, there are also other rotamers and backbone conformations fit into the wrong local  
290 minimum and thus difficult to correct by minimization refinement methods, but not always flagged by  
291 C $\beta$  deviations or other outliers. Some of these, such as *cis*-nonPro peptides (Williams, Videau *et al.*,  
292 2018) or very rare rotamers (Hintze *et al.*, 2016) can be avoided by considering their highly  
293 unfavorable prior probabilities. Others would require explicit sampling of the multiple minima.

### 294 **3.2.3. Lower resolution: peptide orientations with CaBLAM and C $\beta$ d outliers**

295 At low resolution (2.5–4Å), no waters or alternates are modeled. All other problems continue, but an  
296 additional set of common local misfittings occur because the broad electron density is compatible  
297 with significantly different models. 1xgo at 3.5Å is an excellent case for testing in this range, because  
298 it was solved independently from the 1.75Å 1xgs structure – the same molecule in a different space  
299 group. CDL/E&H refinement shows no C $\beta$ d outliers, but Amber refinement has six. Comparison with  
300 1xgs shows that each of the C $\beta$ d residues has either the side chain or the backbone or both in an  
301 incorrect local-minimum conformation uncorrectable by minimization refinement methods  
302 (Richardson & Richardson, 2018). For example, figure 8 shows Leu 253 on a helix, with a C $\beta$ d from  
303 Amber (panel c) and the different, correct 1xgs Leu rotamer in panel d. Those C $\beta$ d outliers are thus a  
304 feature, not a bug, in Amber: they serve their designed validation function of flagging genuine fitting

305 problems. However, the lack of C $\beta$ d outliers in the CDL/E&H refinement is also not a defect, because  
306 the tight CDL/E&H geometry is on average quite useful at low resolution.

307 The 1xgo-vs-1xgs comparison also illustrates many of the ways in which Amber refinement is  
308 superior at low resolution. In figure 8, Amber corrects a Ramachandran outlier in the helix and shows  
309 a helix backbone shape much closer to the ideal geometry of 1xgs than either the deposited or the  
310 CDL/E&H versions.

311 Since the backbone CO direction cannot be seen at low resolution, the commonest local misfitting is a  
312 misoriented peptide (Richardson *et al.*, 2018). Those can be flagged by the new MolProbity validation  
313 called CaBLAM, which tests whether adjacent CO directions are compatible with the local C $\alpha$   
314 backbone conformation (Williams, Headd *et al.*, 2018). Ten such cases were identified in 1xgo, for  
315 isolated single or double CaBLAM outliers surrounded by correct structure as judged in 1xgs. For six  
316 of those 10 cases, neither CDL/E&H nor Amber refinement corrected the problem: His62, Thr70,  
317 Gly163, Gly193, Ala217, Glu286 (see stereo figure S2). In two cases CDL/E&H had fewer other  
318 outliers than Amber, but did not actually reorient the CO: for Gly193 and for the Gly163 case shown  
319 in figure S3. In three of the 10 cases Amber did a complete fix, while CDL/E&H did not improve  
320 (Asp88, Gly125, Pro266). For example, in figure 9, 1xgo residues 86-91 (panel a) have a CaBLAM  
321 outlier (magenta lines), uncorrected by CDL/E&H refinement (panel b). But Amber refinement (panel  
322 c) manages to shift several CO orientations by modest amounts (red balls), enough to fix the  
323 CaBLAM outliers and match extremely closely the better backbone conformation of 1xgs (panel d).  
324 The Gly 125 example is shown in figure S4. Finally, in one especially interesting case (Lys22) Amber  
325 turned the CO about halfway up to where it should be, while CDL/E&H made no improvement. The  
326 Amber model still has geometry outliers and further runs moved most of the way up and removed  
327 those outliers, showing that Amber refinement had not yet fully converged in 10 macrocycles (see  
328 Supplement text and figure S5).

329 Amber refinement is especially good at optimizing hydrogen-aware all-atom sterics, as calculated by  
330 the Probe program (Word, Lovell, LaBean *et al.*, 1999) with H atoms added and optimized by Reduce  
331 (Word, Lovell, Richardson *et al.*, 1999). This is illustrated in figure 10 for 3g8L at 2.5Å resolution.  
332 The deposited structure of the Asn 182 helix N-cap region, which has many outliers of all kinds  
333 (panel a), is improved a great deal by CDL/E&H refinement (panel b). However, the Amber  
334 refinement (panel c) is noticeably better, with more H-bonds and better van der Waals contacts as well  
335 as fewer clashes. These improvements are plotted quantitatively in figure 11, as measured by a  
336 dramatic drop in unfavorable clash spikes (red) and small overlaps (yellow), with a dramatic increase  
337 in favorable H-bonds (green) and van der Waals contacts (blue).

#### 338 4. Discussion

339 The idea of including molecular mechanics force fields into crystallographic refinements is not a new  
340 one, with precedents dating back to early work by (Jack & Levitt, 1978) and the XPLOR program  
341 (Brünger & Karplus, 1991) developed in the 1980's. The notion that a force field could (at least in  
342 principle) encode "prior knowledge" about protein structure continues to have a strong appeal and  
343 efforts to replace conventional "geometric restraints", which are very local and uncorrelated, with a  
344 more global assessment of structural quality have been explored repeatedly (e. g., Moulinier *et al.*,  
345 2003; Schnieders *et al.*, 2009). Distinguishing features of the current implementation include  
346 automatic preparation of force fields for many types of biomolecules, ligands and solvent components  
347 as well as close integration with Phenix, a mature and widely used platform for refinement. This has  
348 enabled parallel refinements on more than 22,000 protein entries in the PDB and allows  
349 crystallographers to test these ideas on their own systems by simply adding flags to an existing  
350 *phenix.refine* command line or adding the same information via the Phenix GUI. Indeed, we expect  
351 most users to "turn on" Amber restraints after having carried out a more conventional refinement to  
352 judge for themselves the significance and correctness of structural differences that arise. As noted in  
353 Section 3.2, an Amber refinement will often flag residues that need manual refitting in ways  
354 complementary to the cues provided by more conventional refinement.

355 The results presented here show that structures with improved local quality (as monitored by  
356 MolProbity criteria and hydrogen bond analysis) can be obtained by simple energy minimization, with  
357 minimal degradation in agreement with experimental structure factors and with no changes to a  
358 current-generation protein force field. Nevertheless, one should keep in mind that the Amber-refined  
359 structures obtained here are not very different from those found with more conventional refinement.  
360 Both methods require that most local misfittings to be corrected in advance. The hope is that either  
361 sampling of explicit alternatives or else optimization using more aggressive conformational search,  
362 such as with simulated annealing or torsion-angle dynamics, may find the correct low-energy  
363 structures with good agreement with experimental data.

364 It is likely that further exploration of relative weights between "X-ray" and "energy" terms (beyond  
365 the existing and heuristic weight-optimization procedure employed here) and even within the energy  
366 terms, will become important. In principle, maximizing the joint probability arising from "prior  
367 knowledge" (using a Boltzmann distribution,  $\exp(-E_{\text{AmberFF}}/k_{\text{B}}T)$  for some effective temperature) and a  
368 maximum likelihood target function (based on a given model and the observed data) is an attractive  
369 approach that effectively establishes an appropriate relative weighting. More study will be needed to  
370 see how well this works in practice, especially in light of the inevitable limitations of current force  
371 fields.

372 The integration of Amber's force field into the Phenix software for crystallography also paves the way  
373 for the development of more sophisticated applications. The force field can accommodate alternate  
374 conformers by using the locally enhanced sampling (LES) approach (Roitberg & Elber, 1991;

375 Simmerling *et al.*, 1998); a few examples are discussed here whilst details will be presented  
376 elsewhere. Ensemble refinement (Burnley *et al.*, 2012) could now be performed using a full molecular  
377 dynamics force field, thus avoiding poor quality individual models in the ensemble. Similarly,  
378 simulated annealing could now be performed with an improved physics-based potential. Extension of  
379 the ideas presented to real-space refinement within Phenix is underway, opening a path to new  
380 applications to cryo-EM and low-resolution X-ray structures. These developments would all  
381 contribute significantly to the future of macromolecular crystallography, reinforcing the transition  
382 from a single static-structure-dominated view of crystals to one where dynamics and structural  
383 ensembles play a central important role in describing molecular function (Furnham *et al.*, 2006; van  
384 den Bedem & Fraser, 2015; Wall *et al.*, 2014).

## 385 **5. Conclusions**

386 We have presented refinement results obtained by integrating Phenix with the Amber software  
387 package for molecular dynamics. Our refinements of over 22,000 crystal structures show that  
388 refinement using Amber's all atom molecular mechanics force field outperforms CDL/E&H restraint  
389 refinement in many respects. An overwhelming majority of Amber-refined models display notably  
390 improved model quality. The improvement is seen across most indicators of model quality including  
391 clashes between atoms, side chain rotamers and peptide backbone torsion angles. In particular,  
392 Phenix-Amber consistently outperforms standard Phenix refinement in clashscore, number of  
393 hydrogen bonds and MolProbity score. It also consistently outperforms standard refinement for  
394 Ramachandran and rotamer statistics at low resolutions and obtains approximately equal results at  
395 high (better than 2.0Å) resolutions. Amber does run somewhat more slowly (generally 20-40%  
396 longer) and may take more cycles to converge completely if it is making any large local changes (see  
397 text for supplementary figure S5). It should be noted that standard refinement consistently  
398 outperforms Phenix-Amber in eliminating C $\beta$  deviation and other covalent-geometry outliers across  
399 all resolutions, but in many cases the Amber outliers serve to flag a real problem in the model.

400 As the quality of experimental data decreases with resolution, the improvement in model quality  
401 obtained by using Amber, as opposed to CDL/E&H restraints, increases. This improvement is  
402 especially striking in the case of clashscores, which appear to be nearly independent of experimental  
403 data resolution for Amber refinements. Additional improvement is seen in the modelling of  
404 electrostatic interactions, H-bonds and van der Waals contacts, which are currently ignored by  
405 conventional restraints. Improving lower-resolution structures is very important, since they include a  
406 large fraction of the most exciting and biologically important current structures such as the  
407 protein/nucleic acid complexes of big, dynamic molecular machines.

408 No minimization refinement method, including CDL/E&H and Amber, can in general correct local  
409 misfittings that were modeled in an incorrect local-minimum conformation, especially at relatively

410 high resolutions. At lower resolution where the barriers are softer, Amber sometimes can manage  
411 such a change, while CDL/E&H still does not. It is, therefore, important and highly recommended that  
412 validation flags be consulted for the initial model and as many as feasible of the worst cases be fixed,  
413 before starting the cycles of automated refinement with either target.

414 **Software distribution** Amber was implemented in *phenix.refine* and is available in the 1.16-3549  
415 version of Phenix and later. Instructions for using the *phenix.refine* Amber implementation are  
416 available in the version-specific documentation available with the distribution.

417 **Acknowledgements** JSR thanks David Richardson for help with some aspects of the individual-  
418 example analyses. The content is solely the responsibility of the authors and does not necessarily  
419 represent the official views of the National Institutes of Health, NIGMS, or DOE.

## 420 **References**

421 Adams, P. D., Afonine, P. V., Bunkóczi, G., Chen, V. B., Davis, I. W., Echols, N., Headd, J.  
422 J., Hung, L.-W., Kapral, G. J., Grosse-Kunstleve, R. W., McCoy, A. J., Moriarty, N.  
423 W., Oeffner, R., Read, R. J., Richardson, D. C., Richardson, J. S., Terwilliger, T. C. &  
424 Zwart, P. H. (2010). *Acta Crystallogr Sect D*. **66**, 213–221.

425 Adams, P. D., Pannu, N. S., Read, R. J. & Brünger, A. T. (1997). *Proc. Natl. Acad. Sci.* **94**,  
426 5018–5023.

427 Afonine, P. V., Echols, N., Grosse-Kunstleve, R. W., Moriarty, N. W. & Adams, P. D.  
428 (2011). *Comput. Crystallogr. Newsl.* **2**, 99–103.

429 Afonine, P. V., Grosse-Kunstleve, R. W., Echols, N., Headd, J. J., Moriarty, N. W.,  
430 Mustyakimov, M., Terwilliger, T. C., Urzhumtsev, A., Zwart, P. H. & Adams, P. D.  
431 (2012). *Acta Crystallogr Sect D*. **68**, 352–367.

432 Agarwal, R. C. (1978). *Acta Crystallogr. Sect. A*. **34**, 791–809.

433 van den Bedem, H. & Fraser, J. S. (2015). *Nat. Methods*. **12**, 307–318.

434 Berman, H. M., Westbrook, J., Feng, Z., Gilliland, G., Bhat, T. N., Weissig, H., Shindyalov,  
435 I. N. & Bourne, P. E. (2000). *Nucleic Acids Res.* **28**, 235–242.

436 Bowman, G. R., Voelz, V. A. & Pande, V. S. (2011). *J. Am. Chem. Soc.* **133**, 664–667.

437 Bricogne, G., Blanc, E., Brandl, M., Flensburg, C., Keller, P., Paciorek, W., Roversi, P.,  
438 Sharff, A., Smart, O. S., Vonrhein, C. & Womack, T. O. (2011).

439 Brünger, A. T. & Karplus, M. (1991). *Acc. Chem. Res.* **24**, 54–61.

440 Brünger, A. T., Karplus, M. & Petsko, G. A. (1989). *Acta Crystallogr. Sect. A*. **45**, 50–61.

441 Brünger, A. T., Kuriyan, J. & Karplus, M. (1987). *Science*. **235**, 458–460.

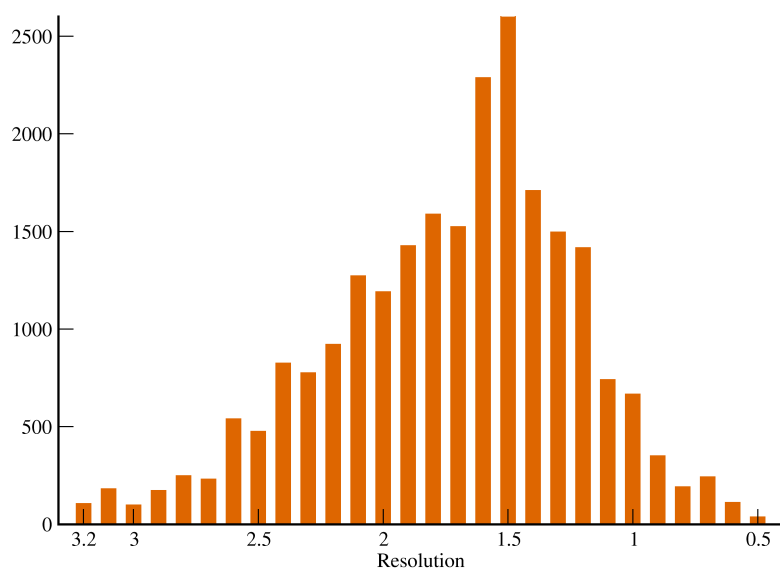
- 442 Burley, S. K., Berman, H. M., Bhikadiya, C., Bi, C., Chen, L., Costanzo, L. D., Christie, C.,  
443 Duarte, J. M., Dutta, S., Feng, Z., Ghosh, S., Goodsell, D. S., Green, R. K.,  
444 Guranovic, V., Guzenko, D., Hudson, B. P., Liang, Y., Lowe, R., Peisach, E.,  
445 Periskova, I., Randle, C., Rose, A., Sekharan, M., Shao, C., Tao, Y.-P., Valasatava,  
446 Y., Voigt, M., Westbrook, J., Young, J., Zardecki, C., Zhuravleva, M., Kurisu, G.,  
447 Nakamura, H., Kengaku, Y., Cho, H., Sato, J., Kim, J. Y., Ikegawa, Y., Nakagawa,  
448 A., Yamashita, R., Kudou, T., Bekker, G.-J., Suzuki, H., Iwata, T., Yokochi, M.,  
449 Kobayashi, N., Fujiwara, T., Velankar, S., Kleywegt, G. J., Anyango, S., Armstrong,  
450 D. R., Berrisford, J. M., Conroy, M. J., Dana, J. M., Deshpande, M., Gane, P.,  
451 Gáborová, R., Gupta, D., Gutmanas, A., Koča, J., Mak, L., Mir, S., Mukhopadhyay,  
452 A., Nadzirin, N., Nair, S., Patwardhan, A., Paysan-Lafosse, T., Pravda, L., Salih, O.,  
453 Sehnal, D., Varadi, M., Vařeková, R., Markley, J. L., Hoch, J. C., Romero, P. R.,  
454 Baskaran, K., Maziuk, D., Ulrich, E. L., Wedell, J. R., Yao, H., Livny, M. &  
455 Ioannidis, Y. E. (2019). *Nucleic Acids Res.* **47**, D520–D528.
- 456 Burnley, B. T., Afonine, P. V., Adams, P. D. & Gros, P. (2012). *ELife*. **1**, e00311.
- 457 Case, D. A., Ben-Shalom, I. Y., Brozell, S. R., Cerutti, D. S., Cheatham, III, T. E., Cruzeiro,  
458 V. W. D., Darden, T. A., Duke, R. E., Ghoreishi, D., Gilson, M. K., Gohlke, H.,  
459 Goetz, A. W., Greene, D., Harris, R., Homeyer, N., Izadi, S., Kovalenko, A.,  
460 Kurtzman, T., Lee, T. S., LeGrand, S., Li, P., Lin, C., Liu, J., Luchko, T., Luo, R.,  
461 Mermelstein, D. J., Merz, K. M., Miao, Y., Monard, G., Nguyen, C., Nguyen, H.,  
462 Omelyan, I., Onufriev, A., Pan, F., Qi, R., Roe, D. R., Roitberg, A., Sagui, C., Schott-  
463 Verdugo, S., Shen, J., Simmerling, C. L., Smith, J., Salomon-Ferrer, R., Swails, J.,  
464 Walker, R. C., Wang, J., Wei, H., Wolf, R. M., Wu, X., Xiao, L., York, D. M. &  
465 Kollman, P. A. (2018). AMBER 18 University of California, San Francisco.
- 466 Cerutti, D. S., Le Trong, I., Stenkamp, R. E. & Lybrand, T. P. (2008). *Biochemistry*. **47**,  
467 12065–12077.
- 468 Cerutti, D. S., Le Trong, I., Stenkamp, R. E. & Lybrand, T. P. (2009). *J. Phys. Chem. B*. **113**,  
469 6971–6985.
- 470 Chen, V. B., Davis, I. W. & Richardson, D. C. (2009). *Protein Sci. Publ. Protein Soc.* **18**,  
471 2403–2409.
- 472 Darden, T., York, D. M. & Pedersen, L. (1993). *J. Chem. Phys.* **98**, 10089.
- 473 Davis, A. M., Teague, S. J. & Kleywegt, G. J. (2003). *Angew. Chem. Int. Ed Engl.* **42**, 2718–  
474 2736.
- 475 Davis, I. W., Arendall, W. B., Richardson, D. C. & Richardson, J. S. (2006). *Struct. Lond.*  
476 *Engl.* **14**, 265–274.
- 477 Engh, R. A. & Huber, R. (1991). *Acta Crystallogr Sect A*. **47**, 392–400.
- 478 Engh, R. A. & Huber, R. (2001). *International Tables for Crystallography. Volume F:*  
479 *Crystallography of Biological Macromolecules*, Vol. edited by M.G. Rossmann & E.  
480 Arnold, pp. 382–392. Dordrecht: Kluwer.

- 481 Furnham, N., Blundell, T. L., DePristo, M. A. & Terwilliger, T. C. (2006). *Nat. Struct. Mol.*  
482 *Biol.* **13**, 184–185.
- 483 Grindon, C., Harris, S., Evans, T., Novik, K., Coveney, P. & Laughton, C. (2004). *Philos.*  
484 *Trans. R. Soc. Lond. Ser. Math. Phys. Eng. Sci.* **362**, 1373–1386.
- 485 Groom, C. R., Bruno, I. J., Lightfoot, M. P. & Ward, S. C. (2016). *Acta Crystallogr. Sect. B*  
486 *Struct. Sci. Cryst. Eng. Mater.* **72**, 171–179.
- 487 van Gunsteren, W. F., Dolenc, J. & Mark, A. E. (2008). *Curr. Opin. Struct. Biol.* **18**, 149–  
488 153.
- 489 Hendrickson, W. A. & Konnert, J. H. (1980). *Computing in Crystallography*, Vol. edited by  
490 R. Diamond, S. Ramaseshan & K. Venkatesan, pp. 13.01–13.26. Bangalore: Indian  
491 Academy of Sciences.
- 492 Hintze, B. J., Lewis, S. M., Richardson, J. S. & Richardson, D. C. (2016). *Proteins-Struct.*  
493 *Funct. Bioinforma.* **84**, 1177–1189.
- 494 Jack, A. & Levitt, M. (1978). *Acta Crystallogr. Sect. A.* **34**, 931–935.
- 495 Janowski, P. A., Cerutti, D. S., Holton, J. M. & Case, D. A. (2013). *J. Am. Chem. Soc.* **135**,  
496 7938–7948.
- 497 Janowski, P. A., Liu, C., Deckman, J. & Case, D. A. (2015). *Protein Sci. Publ. Protein Soc.*
- 498 Liu, C., Janowski, P. A. & Case, D. A. (2015). *Biochim. Biophys. Acta.* **1850**, 1059–1071.
- 499 Lovell, S. C., Davis, I. W., Adrendall, W. B., de Bakker, P. I. W., Word, J. M., Prisant, M.  
500 G., Richardson, J. S. & Richardson, D. C. (2003). *Proteins Struct. Funct. Bioinforma.*  
501 **50**, 437–450.
- 502 Maier, J. A., Martinez, C., Kasavajhala, K., Wickstrom, L., Hauser, K. & Simmerling, C.  
503 (2015). *J. Chem. Theory Comput.* **11**, 150707155125009.
- 504 Moriarty, N. W., Grosse-Kunstleve, R. W. & Adams, P. D. (2009). *Acta Crystallogr. Sect. -*  
505 *Biol. Crystallogr.* **65**, 1074–1080.
- 506 Moriarty, N. W., Tronrud, D. E., Adams, P. D. & Karplus, P. A. (2014). *FEBS J.* **281**, 4061–  
507 4071.
- 508 Moriarty, N. W., Tronrud, D. E., Adams, P. D. & Karplus, P. A. (2016). *Acta Crystallogr.*  
509 *Sect. -Biol. Crystallogr.* **72**, 176–179.
- 510 Moulinier, L., Case, D. A. & Simonson, T. (2003). *Acta Crystallogr. D Biol. Crystallogr.* **59**,  
511 2094–2103.
- 512 Murshudov, G. N., Skubák, P., Lebedev, A. A., Pannu, N. S., Steiner, R. A., Nicholls, R. A.,  
513 Winn, M. D., Long, F. & Vagin, A. A. (2011). *Acta Crystallogr. D Biol. Crystallogr.*  
514 **67**, 355–367.

- 515 Murshudov, G. N., Vagin, A. A. & Dodson, E. J. (1997). *Acta Crystallogr. Sect. D.* **53**, 240–  
516 255.
- 517 Priestle, J. P. (2003). *J. Appl. Crystallogr.* **36**, 34–42.
- 518 Richardson, D. C. & Richardson, J. S. (2001). *Crystallography of Biological*  
519 *Macromolecules*, Vol. *F*, edited by M.G. Rossmann & E. Arnold, p. Dordrecht:  
520 Kluwer Academic Press.
- 521 Richardson, J. S. & Richardson, D. C. (2018). *Comput. Crystallogr. Newsl.* **9**, 21–24.
- 522 Richardson, J. S., Williams, C. J., Videau, L. L., Chen, V. B. & Richardson, D. C. (2018). *J.*  
523 *Struct. Biol.* **204**, 301–312.
- 524 Roe, D. R. & Cheatham, T. E. (2013). *J. Chem. Theory Comput.* **9**, 3084–3095.
- 525 Roitberg, A. & Elber, R. (1991). *J. Chem. Phys.* **95**, 9277–9287.
- 526 Schnieders, M. J., Fenn, T. D., Pande, V. S. & Brunger, A. T. (2009). *Acta Crystallogr. D*  
527 *Biol. Crystallogr.* **65**, 952–965.
- 528 Sheldrick, G. M. (2008). *Acta Crystallogr. Sect. A.* **64**, 112–122.
- 529 Showalter, S. A. & Brüschweiler, R. (2007). *J. Chem. Theory Comput.* **3**, 961–975.
- 530 Simmerling, C., Fox, T. & Kollman, P. A. (1998). *J. Am. Chem. Soc.* **120**, 5771–5782.
- 531 Touw, W. G. & Vriend, G. (2010). *Acta Crystallogr Sect D.* **66**, 1341–1350.
- 532 Tronrud, D. E., Berkholz, D. S. & Karplus, P. A. (2010). *Acta Crystallogr. D Biol.*  
533 *Crystallogr.* **66**, 834–842.
- 534 Tronrud, D. E., Ten Eyck, L. F. & Matthews, B. W. (1987). *Acta Crystallogr. Sect. A.* **43**,  
535 489–501.
- 536 Wall, M. E., Adams, P. D., Fraser, J. S. & Sauter, N. K. (2014). *Struct. Lond. Engl. 1993.* **22**,  
537 182–184.
- 538 Waser, J. (1963). *Acta Crystallogr.* **16**, 1091–1094.
- 539 Williams, C. J., Headd, J. J., Moriarty, N. W., Prisant, M. G., Videau, L. L., Deis, L. N.,  
540 Verma, V., Keedy, D. A., Hintze, B. J., Chen, V. B., Jain, S., Lewis, S. M., Arendall,  
541 W. B., Snoeyink, J., Adams, P. D., Lovell, S. C., Richardson, J. S. & Richardson, D.  
542 C. (2018). *Protein Sci.* **27**, 293–315.
- 543 Williams, C. J., Videau, L. L., Hintze, B. J., Richardson, D. C. & Richardson, J. S. (2018).  
544 *BioRxiv.* 324517.
- 545 Word, J. M., Lovell, S. C., LaBean, T. H., Taylor, H. C., Zalis, M. E., Presley, B. K.,  
546 Richardson, J. S. & Richardson, D. C. (1999). *J. Mol. Biol.* **285**, 1711–1733.



- 547 Word, J. M., Lovell, S. C., Richardson, J. S. & Richardson, D. C. (1999). *J. Mol. Biol.* **285**,  
548 1735–1747.
- 549 York, D. M., Darden, T. A. & Pedersen, L. G. (1993). *J. Chem. Phys.* **99**, 8345–8348.
- 550 Zagrovic, B., Gattin, Z., Lau, J. K.-C., Huber, M. & van Gunsteren, W. F. (2008). *Eur.*  
551 *Biophys. J.* **37**, 903–912.
- 552
- 553

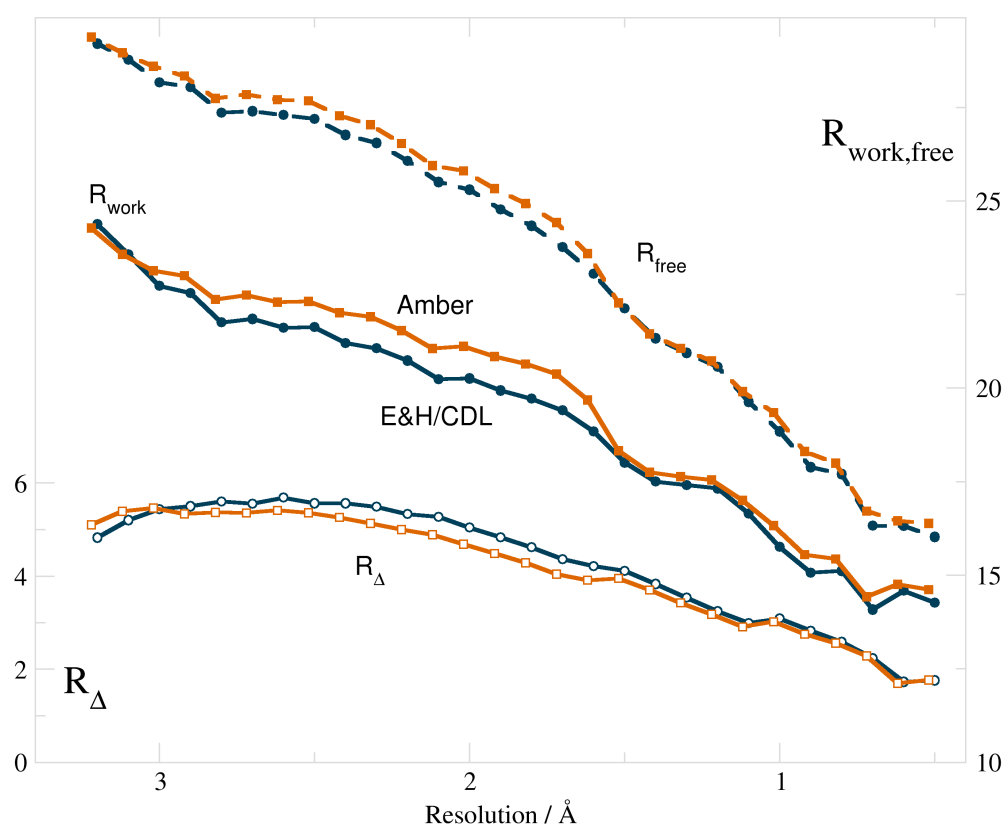


554

555 **Figure 1** Distribution of refined structures across resolution bins.

556

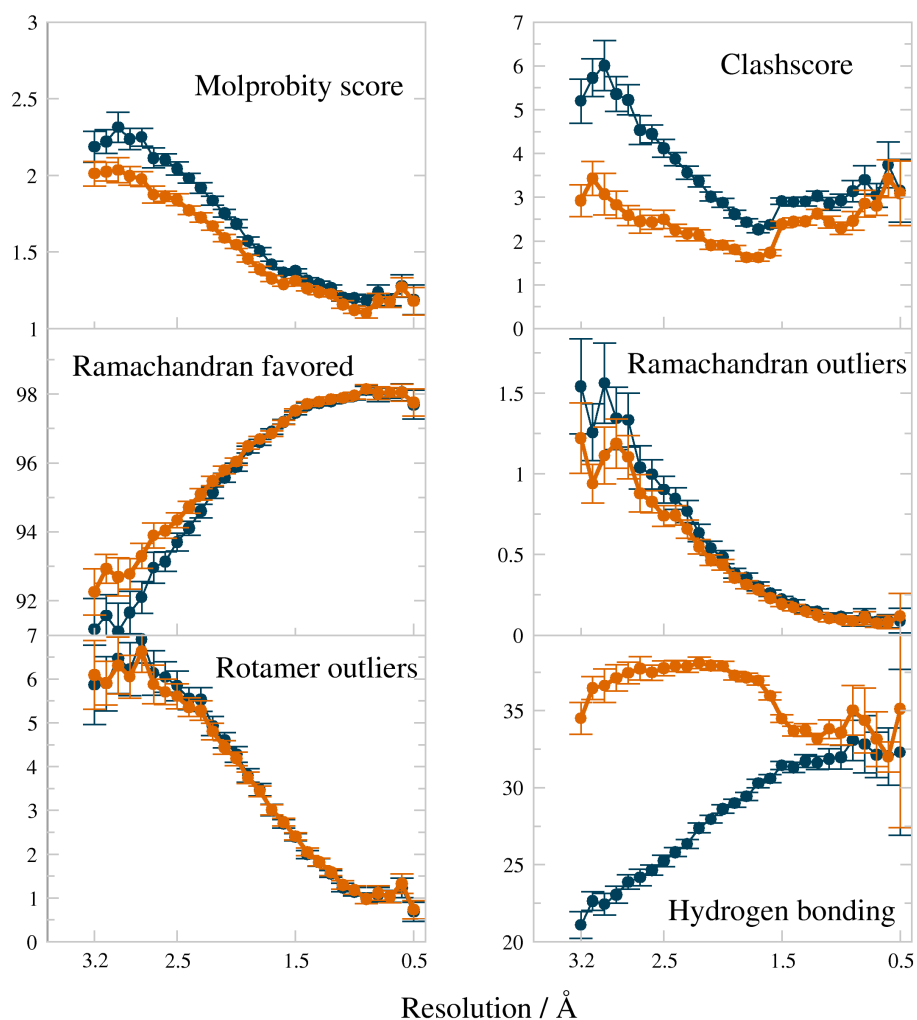
557



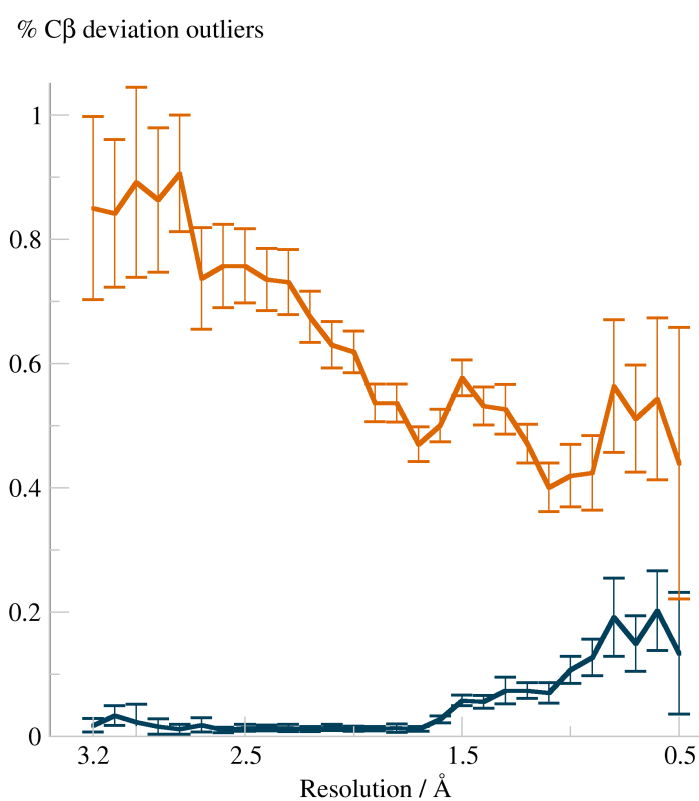
558

559 **Figure 2** R-factors of optimized weight refinements and Rfree-Rwork ( $R_{\Delta}$ ), versus resolution  
560 (values averaged in each resolution bin). Vertical axes are in % with  $R_{\Delta}$  axis on the left. E&H/CDL  
561 values are plotted in dark blue and Amber in burnt orange.

562



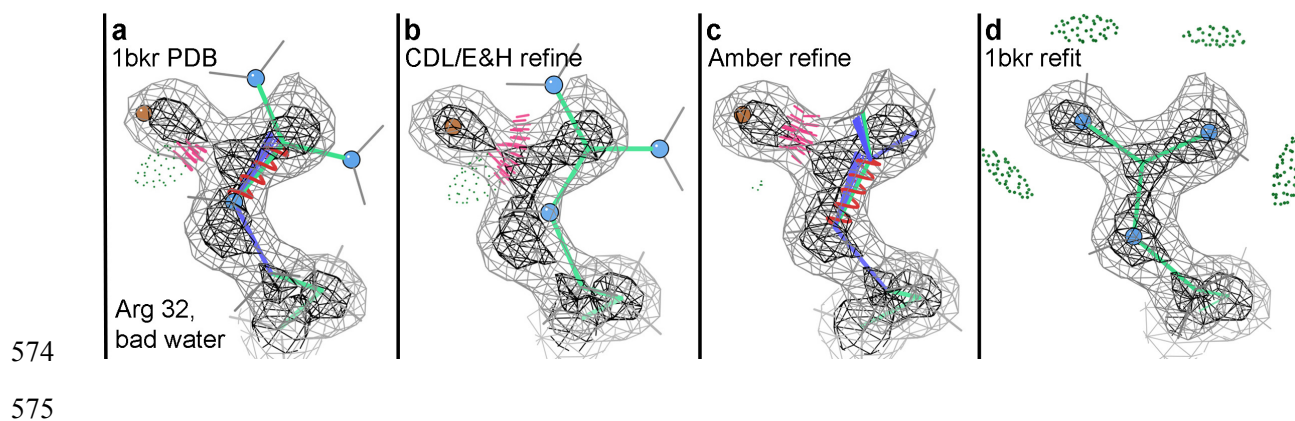
563 **Figure 3** Comparison plots of model quality measures vs resolution, for Amber vs CDL/E&H  
564 refinements with error bars depicting the 95% confidence level of the standard error of the mean.  
565 MolProbity score is a combination of all-atom clashscore, Ramachandran favored and rotamer  
566 outliers, weighted to approximate the expected score at the structure's resolution. The hydrogen bond  
567 fraction is calculated using *cpptraj* per 1000 atoms in the model. For all 6 plots, Amber (burnt orange)  
568 differs in the better direction.



569

570 **Figure 4** Fraction of Cβ deviations (in %) per Cβ atoms as a function of resolution, for the  
571 CDL/E&H (dark blue) and Amber (burnt orange) refinements. Values are averaged in each bin of  
572 resolution, with the error bars showing the 95% confidence level of the standard error of the mean.

573



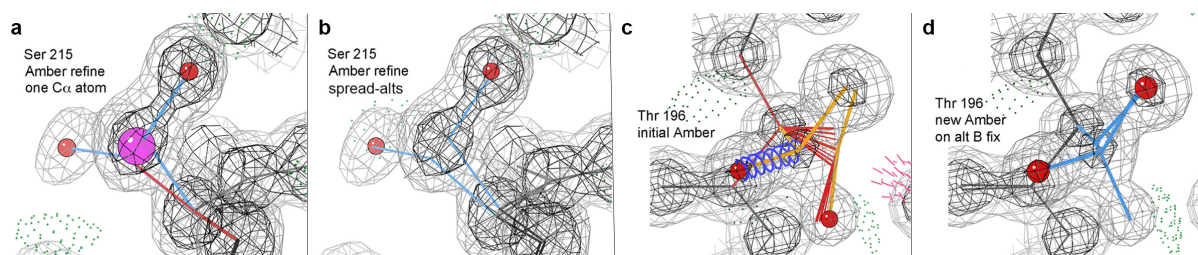
576 **Figure 5** Differing responses of CDL/E&H versus Amber refinement to the misfitting of a water  
577 into what should be a side chain N atom in an Arginine. Neither result here is acceptable, but if the  
578 incorrect water is deleted (panel d), both methods do a very good job of moving the guanidinium  
579 correctly back into its density.

580

581

582

583

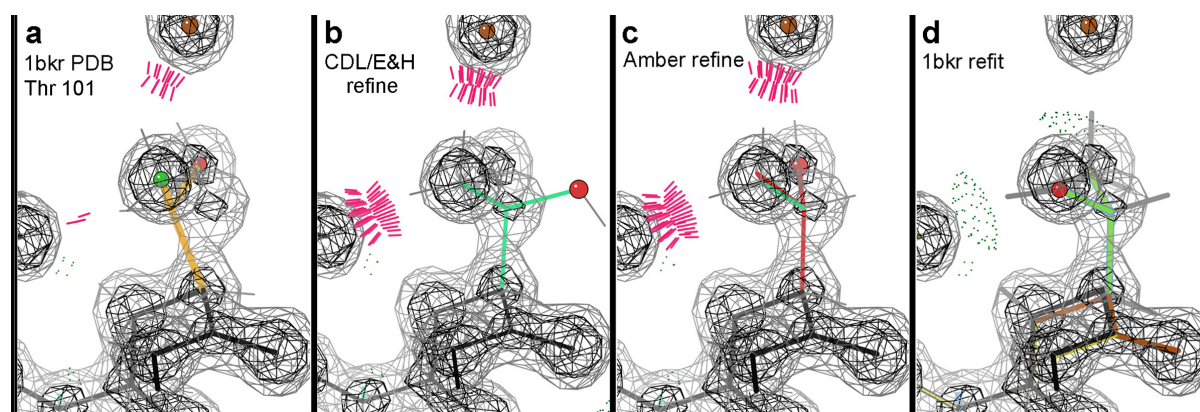


584 **Figure 6** At high resolution, C $\beta$  deviation outliers are most often due to problems with alternate  
585 conformations. a) Amber refinement using the original Ser 215 alternates in PDB file 1nLs, which  
586 have widely separated positions for C $\beta$  but only a single C $\alpha$  atom. b) Amber refinement after the  
587 definition of alternates has been spread to include the C $\alpha$  and both adjoining peptides. c) Amber  
588 refinement of the original Thr 196 of 1nLs, where alternate B had been fit backward; there is bad  
589 covalent geometry and a huge C $\beta$ d of 0.88Å (ball not shown). d) Good Amber result after altB was  
590 refit in the correct rotamer, so that all atoms match the density.

591

592

593



594

595

596 **Figure 7** Unacceptable ways to get rid of a Cβ deviation without fixing the actual problem. a) 1bkr  
597 Thr 101 as deposited, with a huge Cβd of 0.63Å (not shown as a ball because it obscures the side  
598 chain), clashes, a rotamer outlier, the heavier Oγ branch in the lower electron-density peak and the Cβ  
599 out of density -- all caused by modeling the side chain  $\chi_1$  180° backwards. b) CDL/E&H makes the  
600 geometry perfect but puts the Oγ far out of density. c) Amber gets all 3 side chain atoms into peaks by  
601 making the chirality at Cβ incorrect. d) A refit in the correct rotamer replaces clashes with H-bonds,  
602 has no outliers and puts each atom into its correct density peak.

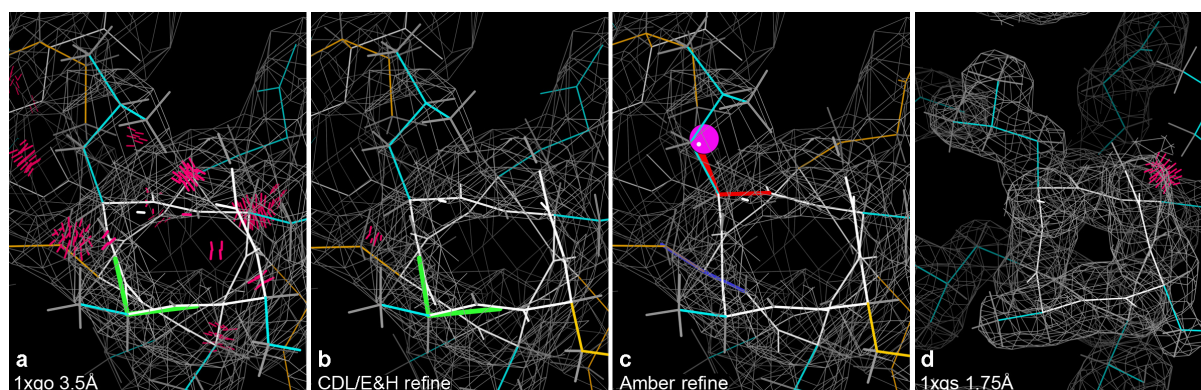
603

604



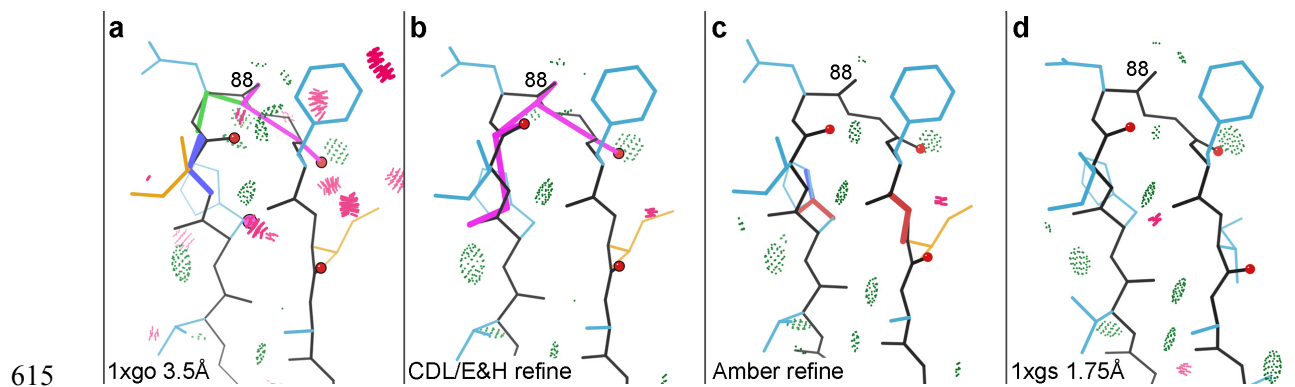
605

606

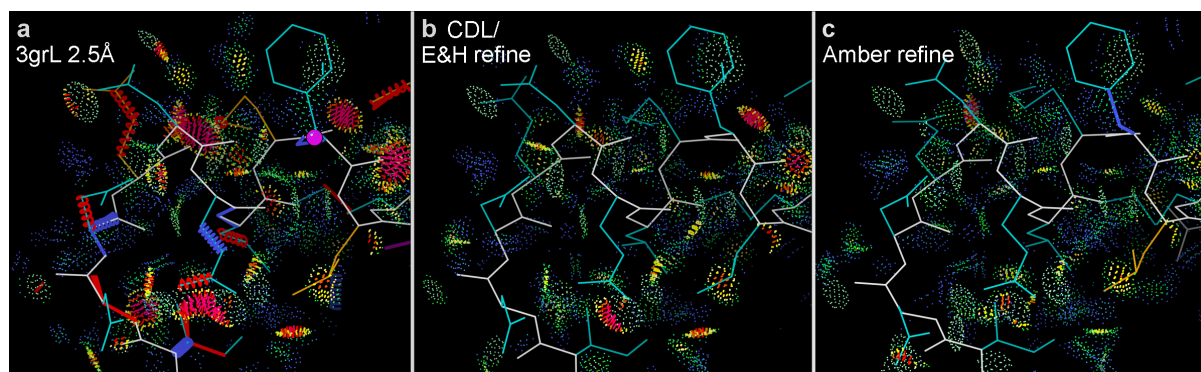


607 **Figure 8** A C $\beta$  deviation in the Amber results at 3.5Å, but not for either the original or the CDL  
608 results. a) 1xgo Leu 253 on a quite distorted helix, with many clashes and a Ramachandran outlier; the  
609 Leu rotamer is incorrect, as shown by the 1xgs structure at 1.75Å. b) CDL/E&H refinement fixes the  
610 clashes, but not the rotamer or Ramachandran outliers or the helix distortion. c) Amber refinement  
611 fixes the clashes and the Ramachandran outlier, flags the incorrect Leu rotamer with a C $\beta$ d outlier and  
612 moves the helix conformation closer to ideal. d) Leu 253 in 1xgs at 1.75Å, with a clearly correct  
613 rotamer on an ideal helix and no outliers besides one clash.

614



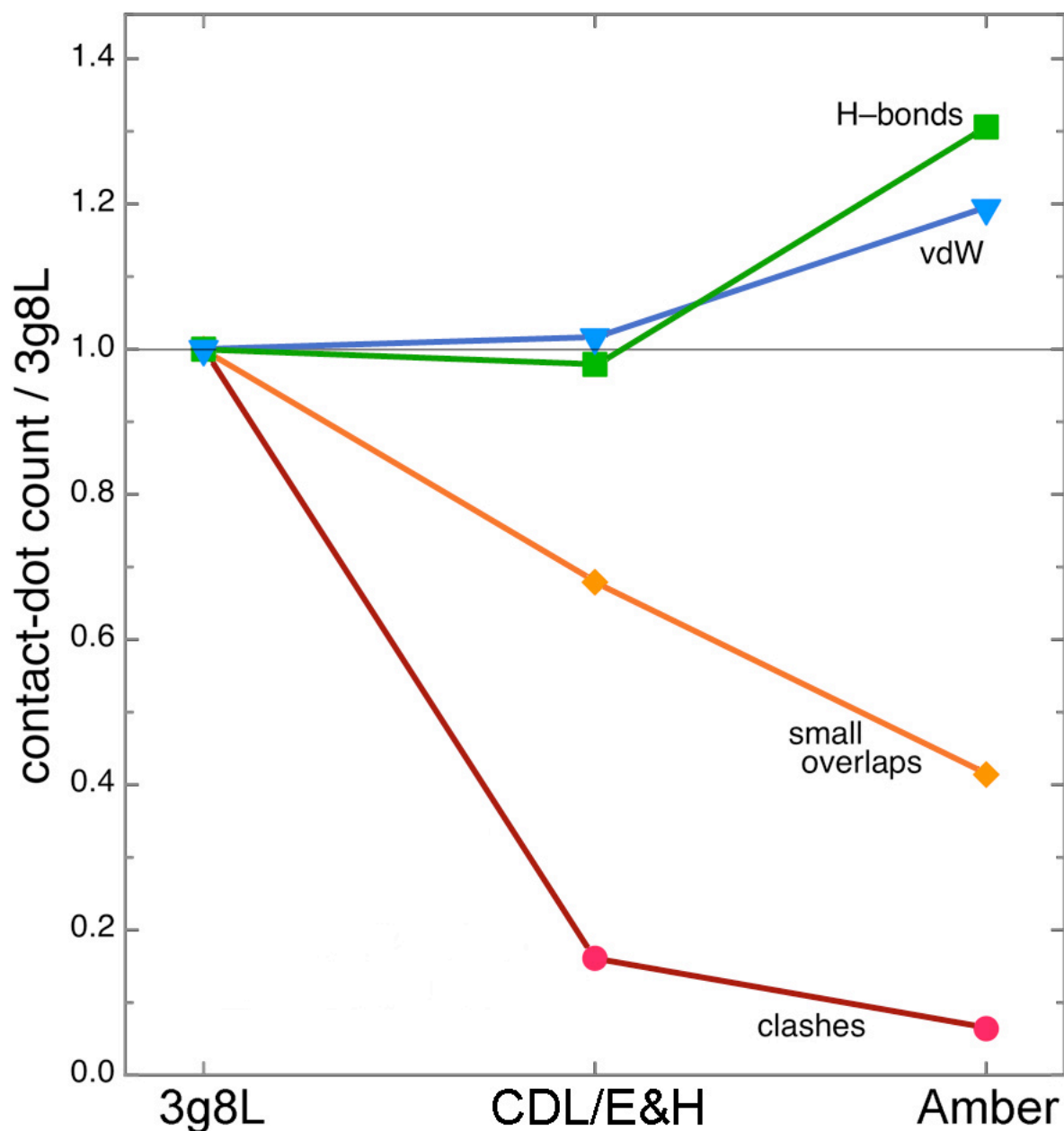
616 **Figure 9** Two misoriented peptides in 1xgo, flagged by Ramachandran and CaBLAM outliers  
617 (magenta outlines on the CO virtual dihedrals). a) Residues 86-91 in the deposited 1xgo structure. b)  
618 CDL/E&H result, with unchanged conformation and outliers. c) Amber result, with several peptide  
619 orientations changed by modest amounts (red balls on CO), removing the backbone outliers and very  
620 closely matching the conformation for 1xgs shown in panel d.



621

622 **Figure 10** Amber refinement produces better H-bonds and van der Waals contacts as well as  
623 removing somewhat more steric clashes. a) The Asn 182 helix-cap region in PDB file 3g8L at 2.5Å,  
624 with numerous clashes and other outliers. b) CDL/E&H refinement makes large improvements,  
625 removing most clashes and all other outliers. c) Amber refinement does even better, removing all  
626 clashes and most small overlaps (yellow) and optimizing to produce more H-bonds and favorable van  
627 der Waals contacts (green and blue dots).

628



629

630 **Figure 11** CDL/E&H versus Amber improvements in steric contacts for the 3g8L helix-cap,  
631 quantified by all-atom contact dot or spike counts measured in Mage (Richardson 2001), normalized  
632 relative to the counts in the deposited 3g8L structure. Amber changes farthest, in the right direction,  
633 for all four contact types.

634

635

## 636 **Supporting information**

### 637 **S1. Full-dataset comparisons**

638 Bond and angle rmsd comparisons (see figure S1) show that the bond rmsd values are numerically  
639 different but are smaller than the average sigma of 0.02Å (2pm) applied to protein bond restraints.  
640 Furthermore the Amber angle rmsd values are approximately 2° across all resolutions – also lower  
641 than the average of ~3° applied to protein angle restraints. The increased CDL/E&H rmsd values at  
642 high resolution may be result of the looser rmsd limit used past 1.5Å for the weight optimisation  
643 process. Comparing the means of the CDL/E&H and Amber rmsd values is not valid as force fields  
644 use more complex energetics rather than harmonic targets to ideal values.

### 645 **S2. Response to Bad Peptide Orientations**

#### 646 **S2.1. Background**

647 The low-resolution analysis of Cβ deviations in the main text made use of comparing the 1xgo  
648 structure at 3.5Å (Tahirov 1998) versus 1xgs at 1.75Å from the same paper. All six Cβ deviations in  
649 the Amber results versus none from CDL/E&H were compared, finding that in each case that Cβd  
650 was flagging an underlying problem: either a misfit side chain or an incompatibility between  
651 backbone and side chain.

652 For the issue of bad peptide orientations, however, only one example was illustrated (Figure 9). These  
653 problems are common at resolutions worse than 2.5Å, because the backbone CO direction is no longer  
654 seen (Richardson *et al.*, 2018). Misoriented peptides are best diagnosed by CaBLAM (Williams  
655 2018). CaBLAM uses virtual dihedral angles of successive Cαs and of successive COs to test whether  
656 the orientations of successive CO groups are compatible with the surrounding Cα trace. It flags  
657 outliers graphically in magenta on the CO-CO virtual dihedral. Since typically there is an energy  
658 barrier between widely different peptide orientations, the presumption is that refinement cannot easily  
659 correct these cases. However, that presumption needs to be tested.

#### 660 **S2.2. Most are not correctable by refinement**

661 Ten cases were identified in 1xgo, for isolated single or double CaBLAM outliers (usually with other  
662 outliers also), surrounded by correct structure as judged in the same molecule at 1.75Å resolution  
663 (1xgs). For 6 of those 10 cases, neither CDL/E&H nor Amber refinement corrected the problem  
664 (His62, Thr70, Gly163, Gly193, Ala217, Glu286).

665 For example, figure S2 shows stereo images of the Glu286-Lys287 hairpin-loop case, where the  
666 CaBLAM outlier in 1xgo is accompanied by clashes, Ramachandran and rotamer outliers. Both

667 CDL/E&H and Amber conformations are essentially identical to the original 1xgo, with no peptide  
668 improvement. They both remove all the clashes (clusters of hotpink spikes) and remove one of the six  
669 side chain outliers (gold) but not into the correct rotamer. In contrast, the high-resolution 1xgs, with  
670 very clear electron density (bottom panel), shows the Lys C $\alpha$  and the two peptide carbonyl oxygens  
671 (red balls) differently placed by large distances and dihedral angles, forming a well H-bonded  $\beta$ -  
672 hairpin with no outliers of any kind.

### 673 **S2.3. Other Outliers Often Better**

674 In two cases the CDL/E&H results had fewer other outliers than Amber, although it did not actually  
675 reorient the peptide CO (Gly163, Gly193). The Gly163 case is shown in stereo in figure S3, for an S-  
676 shaped loop between non-adjacent  $\beta$ -strands, with two CaBLAM flags (magenta) and many other  
677 outliers. Both refinements remove the clashes, one of the rotamer outliers and one of the  
678 Ramachandran outliers (green). The CDL/E&H results in addition removed one of the CaBLAM  
679 outliers and the C $\alpha$ -geometry outlier (red). However, neither refinement could manage the large  
680 rotation needed to correct the 163-164 peptide orientation, as judged by the more convincing  
681 conformation of the high-resolution 1xgs at bottom.

### 682 **S2.4. Amber Sometimes Corrects Well**

683 In three cases Amber managed a complete fix, while in contrast CDL/E&H did not improve (Asp88,  
684 Gly125, Pro266). The Asp88-Gly89 tight turn example is shown in Figure 9 of the main text.

685 Here in figure S4, the Gly125 loop example in a helix-helix connection is shown in stereo, to allow  
686 clear visualization of the CO orientation changes. 1xgo residues 121-126 (figure S3a) have two  
687 CaBLAM outliers (magenta dihedral lines) unchanged by CDL/E&H refinement (panel b). However,  
688 Amber refinement (panel c) manages to shift several CO orientations by up to 80° (red balls), enough  
689 to fix the CaBLAM outliers and to match extremely closely the better backbone conformation of 1xgs  
690 (panel d).

### 691 **S2.5. A Partial Correction, Unconverged**

692 Finally, in one especially interesting case (Lys22, in Figure S5a for 1xgo) Amber turned the CO (red  
693 circles) about halfway up to where it should be (panels b vs c), while CDL/E&H made no  
694 improvement to the peptide. The Amber model eliminated the Ramachandran and one of the  
695 CaBLAM outliers, but still had geometry outliers (a bond angle and a C $\beta$  deviation). It seemed likely  
696 that Amber refinement had not fully converged and might move the CO all the way if run longer.

697 A 30-cycle Amber run had earlier been done for 1xgo, without any major changes noticed beyond the  
698 10-cycle. From that endpoint, two further runs were done, first of 30 cycles ("Amber60"), then a  
699 further 10 cycles ("Amber70").

700 Figure S5d shows the fan of CO positions for all 7 of the deposits and refinements, progressively  
701 rotating counterclockwise from 1xgo to 1xgs. Indeed, both Amber60 and Amber70 successfully  
702 rotated the Lys22 peptide almost all the way to the good helical position seen in the high-resolution  
703 1xsg (panel e), eliminating both the CaBLAM outlier and the intermediate-stage bond-angle outliers,  
704 presumably having crossed an energy barrier in the process.

705 One other CaBLAM-outlier peptide was corrected in Amber70 as well (Thr71). But for the Ala217  
706 outlier, the wrong peptide was rotated, seduced by H-bonding to an Arg side chain in the wrong  
707 position.

708 In these long refinements, both R-factors and match to electron density suffer somewhat. In the cases  
709 examined, this often seems due to incorrect side chain rotamers (almost never correctable by  
710 refinement) pushing an otherwise-good backbone conformation a bit out of density (translated  
711 upward, for 1xgo Lys22). Future work will try to guide early correction of as many problems as  
712 feasible, for the faster and more successful refinement afterward that we now know is possible.

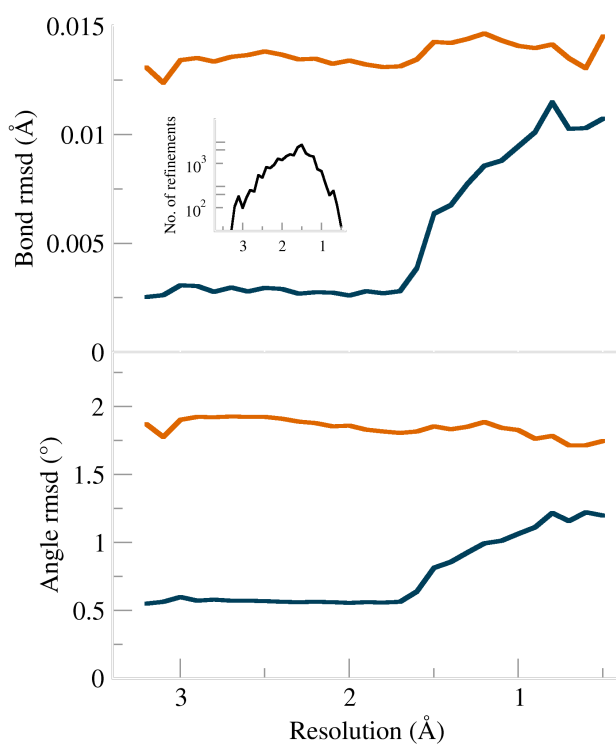
## 713 **S2.6. Discussion**

714 In summary, it is indeed true that refinement cannot usually correct a peptide orientation that is off by  
715 a large amount. The very tight geometry restraints in the CDL/E&H system presumably raise the  
716 barriers to peptide rotation. Amber is rather better at that, and about 1/3 of the time managed a good  
717 correction, although convergence can be very slow for such large changes. We feel it is crucial to try  
718 correcting problems such as flipped peptides in the initial model before refining it, however, crosstalk  
719 between backbone and side chains further complicates that process. However, we are enthusiastic  
720 about use of the Amber target to realistically improve conformation and especially sterics, once the  
721 model is mostly in the right local minima.

## 722 **S2.7. References**

- 723 Richardson J, Richardson D (2018) C $\beta$  deviations and other aspects in Amber versus CDL  
724 refinements, *Comp. Cryst. Newsletter* **9**: 21-24
- 725 Tahirov TH, Oki H, Tsukihara T, Ogasahara K, Yutani K, Ogata K, Izu Y, Tsunasawa S, Kato I  
726 (1998) Crystal structure of methionine aminopeptidase from hyperthermophile *Pyrococcus*  
727 *furiosus*, *J. Mol. Biol.* **284**: 101-124 [1xgo, 1gsx]
- 728 Richardson JS, Williams CJ, Videau LL, Chen VB, Richardson DC (2018) "Assessment of detailed  
729 conformations suggests strategies for improving cryoEM models: helix at lower resolution,  
730 ensembles, pre-refinement fixups, and validation at a multi-residue length scale", *J Struct. Biol.*  
731 **204**: 301-312
- 732 Williams CJ, Hintze BJ, Headd JJ, Moriarty NW, Chen VB, Jain S, Prisant MG, Lewis SM, Videau  
733 LL, Keedy DA, Deis LN, Arendall WB III, Verma V, Snoeyink JS, Adams PD, Lovell SC,  
734 Richardson JS, Richardson DC (2018) MolProbity: More and better reference data for improved  
735 all-atom structure validation, *Protein Sci.* **27**: 293–315 [CaBLAM]

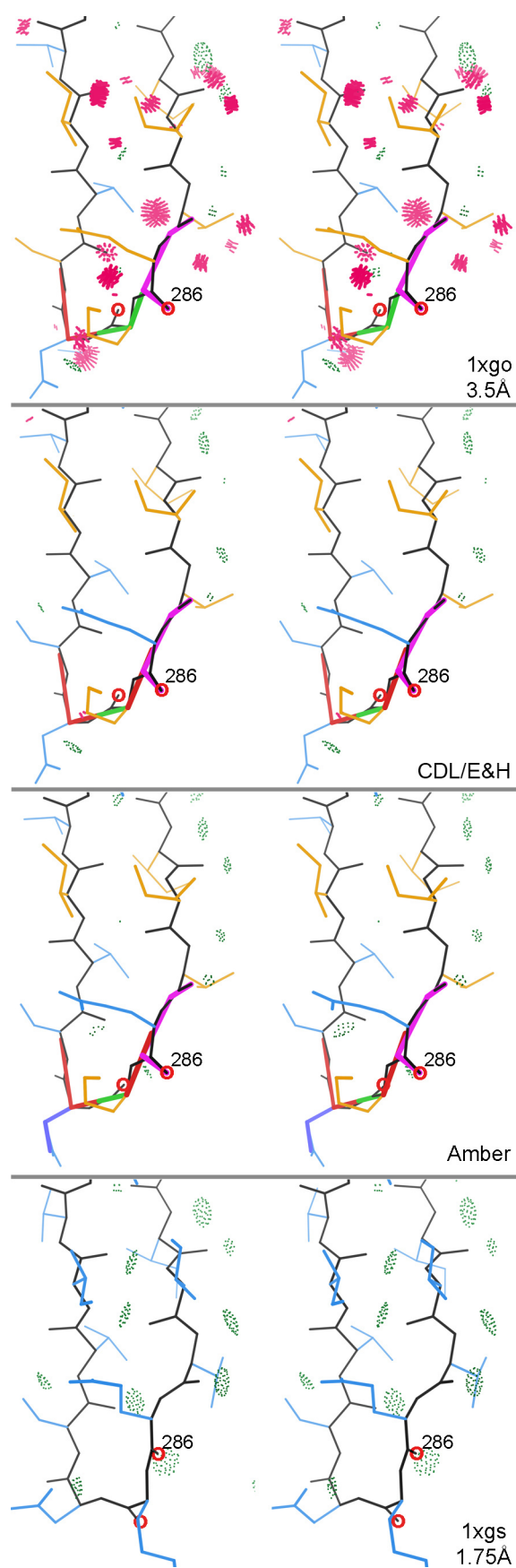
736



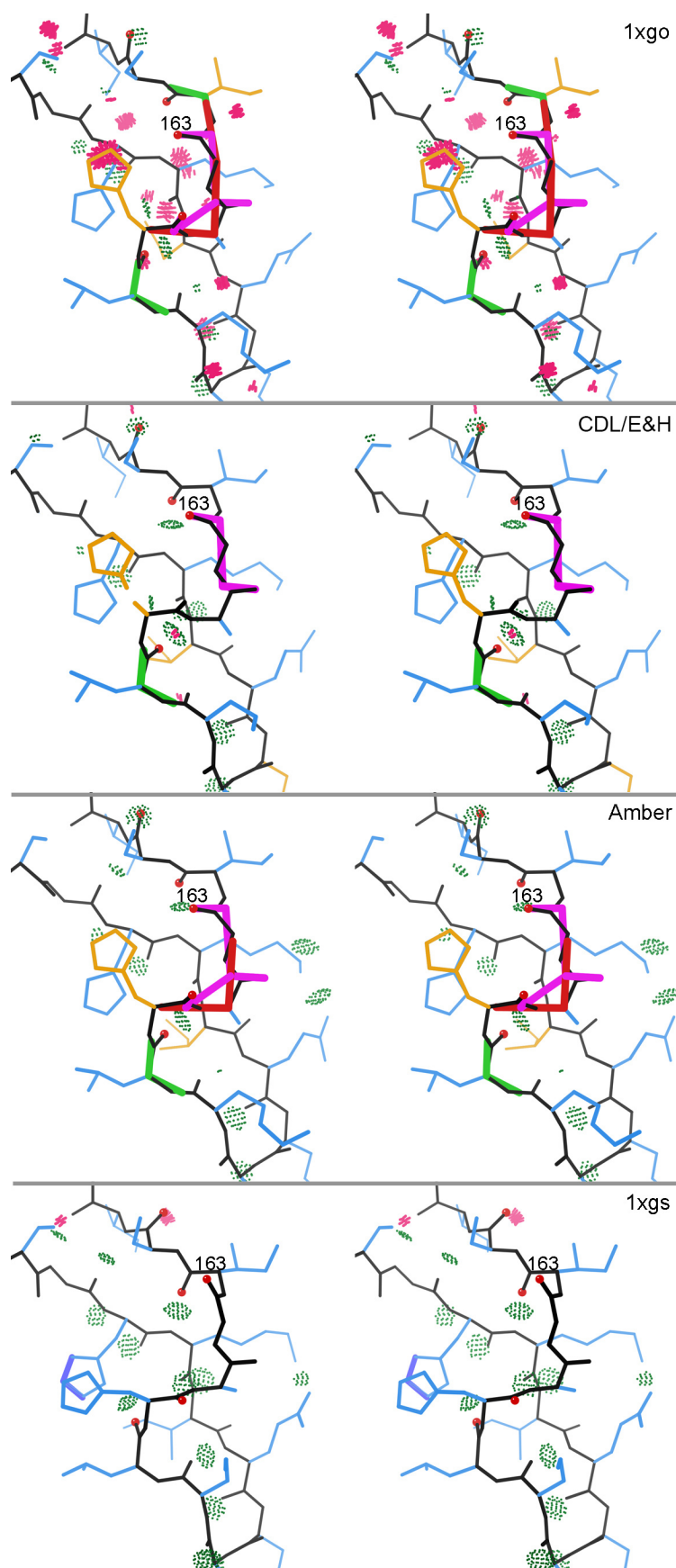
737

738 **Figure S1** Bond and angle rmsd values for CDL/E&H (dark blue) and Amber (burnt orange) plotted  
739 against resolution.

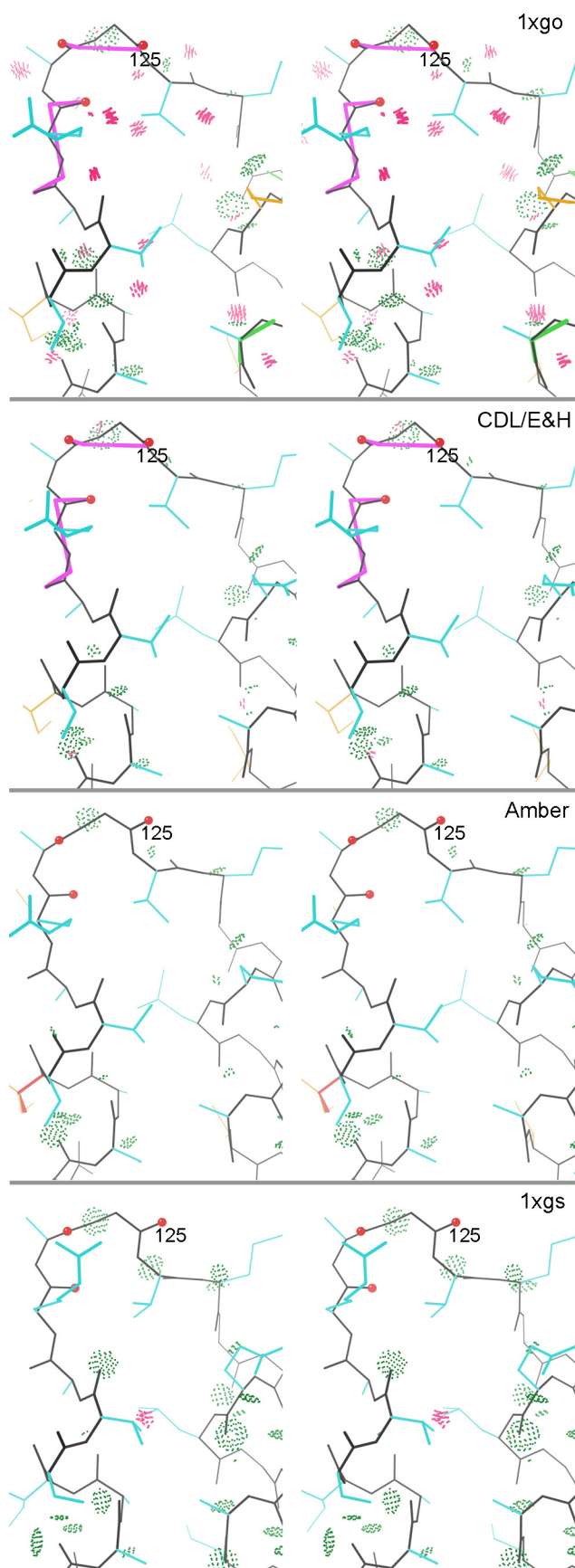




741 **Figure S2** Stereo images of uncorrected CaBLAM problems for the beta-hairpin loop at Glu 286 -  
742 Lys 287 in 1xgo at 3.5Å resolution. a) As deposited, with outliers for CaBLAM (magenta lines on the  
743 CO dihedral), CaBLAM C $\alpha$ -geometry (red lines on C $\alpha$  trace), Ramachandran (green lines along  
744 backbone), rotamer (gold sidechains), and all-atom clash (clusters of hot-pink spikes) evaluations. b)  
745 As refined by Phenix CDL/E&H and c) as refined by Phenix Amber, both of which remove the  
746 clashes but do not correct the underlying conformation. d) In the 1xgs structure at 1.75Å resolution,  
747 showing a classic, outlier-free beta hairpin conformation with good backbone H-bonding and  
748 substantial corrections in peptide orientation and sidechain placement. The 286 and 287 peptide  
749 oxygens that move most are circled in red.

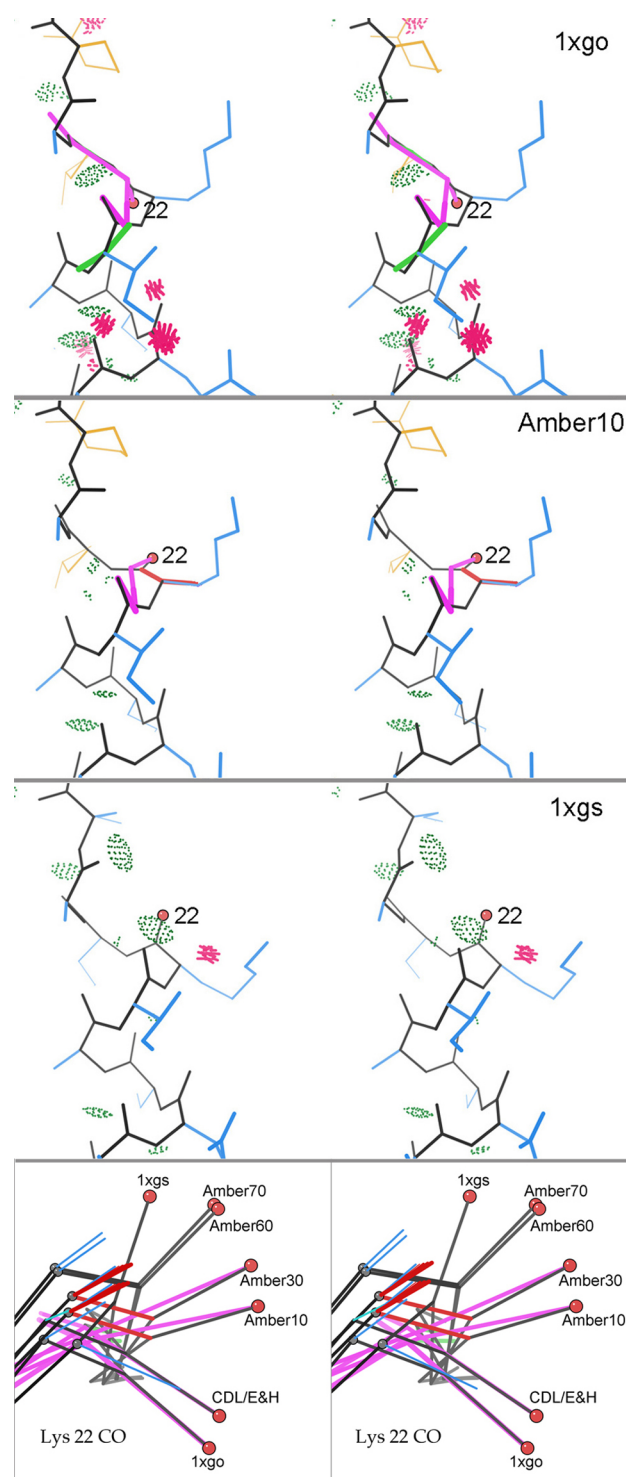


751 **Figure S3** Partial correction of an S-shaped loop at 159-164 in 1xgo. a) As deposited, with many  
752 types of outliers. b) CDL/E&H corrects all but two backbone outliers. c) Amber corrects all clashes  
753 but few other outliers, and neither refinement changes the poor underlying conformation. d) The 1xgs  
754 structure achieves an outlier-free, well H-bonded conformation by shifting 4 peptide orientations (red  
755 ball on carbonyl O atoms), especially at Gly 163.



757 **Figure S4** Successful Amber CaBLAM corrections in the helix-helix loop at 1xgo 121-126. a) As  
758 deposited, with clashes and two CaBLAM outliers. a) CDL/E&H corrects the clashes but not the  
759 backbone conformation. b) Amber reorients 3 successive peptides (red balls on peptide Os) by up to  
760 80°, removing both CaBLAM outliers and matching extremely closely the conformation seen at high  
761 resolution in panel d.

762



763

764 **Figure S5** Gradual correction of the helix C-cap at 1xgo Lys 22. a) As deposited, with double  
765 CaBLAM outliers, clashes, and Ramachandran outlier. CDL/E&H refinement fixes clashes but leaves  
766 conformation unchanged. b) Amber refinement moves the crucial Lys 22 CO partway up toward  $\alpha$ -  
767 helical orientation, relieving one of the CaBLAM outliers. c) Helical, outlier-free conformation of the  
768 C-cap region in 1xgs at high resolution. d) Superposition in side view, showing all Lys 22 CO  
769 orientations between 1xgo outlier and 1xgs  $\alpha$ -helical: longer Amber refinement progressively corrects

770 the orientation, converging close to the 1xgs orientation although with a translational shift we believe  
771 is an effect of incorrect sidechain rotamers.

772

773